

## $^{64}\text{Ni} + ^{92}\text{Zr}$ fission yields at energies close to the Coulomb barrier

F. L. H. Wolfs, R. V. F. Janssens, R. Holzmann,\* T. L. Khoo, W. C. Ma,<sup>†</sup> and S. J. Sanders

*Argonne National Laboratory, Argonne, Illinois 60439*

(Received 11 August 1988)

Fission yields for the  $^{64}\text{Ni} + ^{92}\text{Zr}$  reaction at laboratory energies between 240 and 300 MeV have been measured. "Elastic scattering" angular distributions were also obtained and used to deduce the generalized total reaction cross sections. The competition between fission and light-particle evaporation from the compound nucleus is well reproduced by statistical-model calculations. However, the calculated neutron multiplicities for this reaction are larger than those previously measured. Possible reasons for this discrepancy are discussed.

### I. INTRODUCTION

In several heavy-ion induced fusion reactions, significant deviations have been observed between statistical-model calculations and measurements of the number of nucleons evaporated from the compound nuclei.<sup>1-3</sup> In particular, an extensive set of data exists for the compound nucleus  $^{156}\text{Er}$ , which has been studied with two different entrance channels:<sup>4</sup>  $^{64}\text{Ni} + ^{92}\text{Zr}$  and  $^{12}\text{C} + ^{144}\text{Sm}$ . In the  $^{64}\text{Ni} + ^{92}\text{Zr}$  reaction, the statistical-model calculations overestimate the number of neutrons emitted by an average of 0.4 neutrons over a wide range of excitation energies. In contrast, excellent agreement between the statistical-model calculations and experimental results was found for the neutron multiplicities observed in the  $^{12}\text{C} + ^{144}\text{Sm}$  reaction. For these two entrance channels, data also exist for the evaporation-residue cross sections,<sup>4</sup> the evaporation-residue spin distributions,<sup>5,6</sup> the characteristic neutron and gamma-ray spectra, and multiplicity distributions.<sup>1,7</sup> In the spin-distribution measurement, performed with the Heidelberg-Darmstadt crystal ball, strong differences between the two channels were found for the ratio between two- and three-neutron evaporation at a given excitation energy and spin. Again, the data for the  $^{12}\text{C} + ^{144}\text{Sm}$  are well reproduced by the statistical-model calculations, while large deviations, especially at large angular momenta, are found for the  $^{64}\text{Ni} + ^{92}\text{Zr}$  system. In summary, whereas all of the data available for the  $^{12}\text{C} + ^{144}\text{Sm}$  reaction are consistent with a picture of fusion followed by a statistical decay process, the  $^{64}\text{Ni} + ^{92}\text{Zr}$  system shows anomalous behavior in the neutron evaporation channels. Possible explanations of the apparent inhibition of neutron emission in the  $^{64}\text{Ni} + ^{92}\text{Zr}$  system based on anomalously large neutron energies, large gamma-decay widths, or uncertainties in the location of the yrast line can be ruled out by the available data.<sup>1,4,5</sup>

It has been suggested<sup>8</sup> that the explanation for the inhibition of neutron emission may lie in the presence of high- $l$  tails in the angular momentum distribution for the Ni-induced reaction. By placing more of the compound-nucleus cross section at higher spin values, the effective excitation energy above the yrast line would be reduced,

thus resulting in a lower neutron multiplicity. However, statistical-model calculations suggest that high- $l$  tails of the spin distribution of the compound nucleus mainly contribute to the fission yields and have little effect on the evaporation-residue cross sections. Therefore, a measurement of the competition between fission and evaporation as a function of bombarding energy can be used to test these calculations and to study the shape of the spin distribution. The angular momentum distribution of the compound nucleus obtained in this way is a necessary ingredient for any further statistical-model calculations.

In this paper we present the results of measurements of the fission yields for  $^{64}\text{Ni} + ^{92}\text{Zr}$  at bombarding energies between 240 and 300 MeV, which correspond to energies between 1.05 and 1.30 times the Coulomb barrier [calculated assuming  $R_C = 1.4(A_p^{1/3} + A_t^{1/3})$ ]. The experimental technique used will be discussed in Sec. II. In Sec. III the experimental results will be presented. The decomposition of the total reaction cross sections will be discussed in Sec. IV. The data will be compared with the results of statistical-model calculations, and the possibility of the system becoming trapped in a superdeformed minimum will be studied. The results are summarized in Sec. V.

### II. EXPERIMENTAL METHOD

Beams of 240–300-MeV  $^{64}\text{Ni}$  particles from the Argonne Tandem-Linac Accelerator System (ATLAS) were incident on a  $111\text{-}\mu\text{g}/\text{cm}^2$  isotopically enriched  $^{92}\text{Zr}$  target (97.1%  $^{92}\text{Zr}$ ) evaporated onto a  $20\text{ }\mu\text{g}/\text{cm}^2$  carbon backing. The beam spot on the target was defined by a set of circular collimators to less than 3 mm. Beam currents measured in a Faraday cup behind the target were typically 0.75 particle nA. The stability of the beam and the target quality were monitored on line with three silicon surface barrier detectors. The beam energy was measured using the ATLAS time-of-flight system<sup>9</sup> with an accuracy of better than 0.1 MeV. The effective beam energy was obtained from the measured beam energy after correcting for the energy loss in the target.

The two coincident reaction products were detected in two large-area ( $20 \times 20\text{ cm}^2$ ), position-sensitive, parallel-grid avalanche counters (PGAC's) mounted 40 cm from

the target. At each energy, the fission yields were measured with  $\theta_{\text{PGAC1}} = \theta_{\text{PGAC2}} = 50^\circ$  and with  $\theta_{\text{PGAC1}} = 60^\circ$  and  $\theta_{\text{PGAC2}} = 37.5^\circ$ , relative to the beam direction. Each counter provides a fast timing signal and two-dimensional position information. From the measured scattering angles and the relative time-of-flight, the masses and energies of the two reaction products can be calculated, assuming a two-body final channel. Events were accepted only if the two reaction products were in the reaction plane to within  $\pm 2.5^\circ$ . Those events in which the direction of the reaction products is slightly changed due to the evaporation of light particles are included within the  $\pm 2.5^\circ$  limit. The measured absolute time-of-flight of both reaction products was used to calculate the total mass of the two reaction products. This calculation does not require a knowledge of the actual target mass and was used to reject events originating from target contaminants.

The monitor yields were used for relative normalization between different runs. Absolute cross sections were obtained by normalizing the number of elastic events at the most forward angles to the corresponding Rutherford cross sections. The accuracy of this procedure is estimated to be about 15%. The data were corrected event-by-event for the geometrical detector efficiency which is a function of the detector position and the reaction kinematics.

### III. EXPERIMENTAL RESULTS

#### A. Mass distributions

Fig. 1(a) shows a contour plot of the reaction  $Q$  value versus the mass of the fragment detected in one of the two detectors for  $^{64}\text{Ni} + ^{92}\text{Zr}$  at  $E_{\text{lab}} = 299.1$  MeV. The fission fragments are clearly separated from the elastic, quasielastic, and deep-inelastic fragments. The average  $Q$  value of the fission fragments is  $-62$  MeV and agrees nicely with the predicted  $Q$  value of  $-62.7$  MeV obtained from the Viola systematics.<sup>10</sup> Figure 1(b) shows the mass distribution of events with a reaction  $Q$  value more positive than  $-20$  MeV. The mass resolution obtained at 299.1 MeV is  $\sim 3.5$  u and the energy resolution is  $\sim 10$  MeV. The mass resolution improves with decreasing bombarding energy (2.5 u at 240 MeV) as a result of an increase in the time-of-flight of the reaction products. The mass distribution of fission fragments is shown in Fig. 1(c). Its width (23 u) indicates that at lower bombarding energies problems will arise with the separation between fission and deep-inelastic scattering fragments with mass close to that of the projectile and target. Thus, at the lower bombarding energies ( $E_{\text{lab}} \leq 260$  MeV), only the yields for fission fragments with mass between 75 and 80 u [see Fig. 1(c)] were extracted, and the shape of the fission-fragment mass distribution at 269.8 MeV was used to estimate the total fission yield. This procedure assumes that the shape of the mass distribution of fission fragments does not vary in the energy region studied. This is a reasonable approximation since the square of the width of the mass distribution ( $\sigma_A^2$ ) scales linearly with the nuclear temperature;<sup>11</sup> for the Ni+Zr system in the energy region between 240 MeV and 270 MeV, this

would translate into at most a 15% decrease in the width of the mass distribution between  $E_{\text{lab}} = 269.8$  MeV and  $E_{\text{lab}} = 239.3$  MeV. The uncertainties in the actual width of the fission mass distribution together with the uncertainties in the fission angular distributions (discussed in Sec. III C) are included in the relatively large errors quoted for the total fission yields at the lowest incident energies.

#### B. Elastic scattering

The poor mass and energy resolution obtained in this experiment (Fig. 1) did not allow us to separate elastic scattering from inelastic and quasielastic scattering. Therefore, the elastic scattering yields presented in this paper include contributions from all events with masses close to that of the projectile and target ( $|\Delta m| \leq 7$  u) and with a reaction  $Q$  value more positive than  $-20$  MeV.

Figure 2 shows the measured "elastic scattering" yields divided by the Rutherford cross section as a function of the center-of-mass scattering angle at several incident energies. The solid curves in Fig. 2 show the results of optical-model fits to the data with an energy independent real and imaginary Woods-Saxon potential with parameters  $V = -60$  MeV,  $r_0 = 1.05$  fm,  $a = 0.64$  fm,  $W = -40$  MeV,  $r_{0i} = 1.39$  fm, and  $a_i = 0.24$  fm. The total reaction cross sections obtained from these optical-model calculations are tabulated in Table I. The quality of the fit can

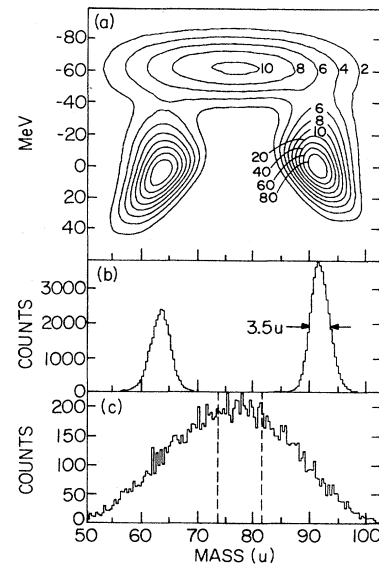


FIG. 1. (a) Contour plot of the yield observed in detector 1 vs the measured reaction  $Q$  value and the mass of the fragment detected in detector 1 for  $^{64}\text{Ni} + ^{92}\text{Zr}$  at  $E_{\text{lab}} = 299.1$  MeV and  $\theta_{\text{PGAC1}} = \theta_{\text{PGAC2}} = 50^\circ$ . (b) Projection of the contour plot shown in (a) onto the mass axis for events with a reaction  $Q$  value more positive than  $-20$  MeV. (c) Projection of the contour plot shown in (a) onto the mass axis for the fission fragments ( $-80$  MeV  $< Q_{\text{reac}} < -40$  MeV). The dashed lines indicate the mass region for which the fission yields were determined at bombarding energies below 270 MeV (see text).

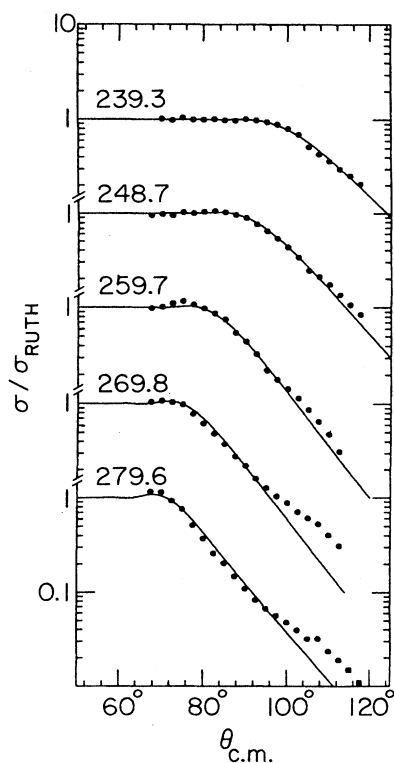


FIG. 2. Measured elastic scattering angular distributions for  $^{64}\text{Ni} + ^{92}\text{Zr}$  at several bombarding energies (indicated are the laboratory energies in MeV). The solid lines show the results of optical-model fits.

be improved by using the real and imaginary radius and diffuseness as free parameters at each energy. The corresponding change in the deduced reaction cross sections is included in the errors quoted in Table I. At the higher bombarding energies the “elastic scattering” cross sections at large center-of-mass angles are significantly larger than the optical-model predictions. The cutoff of

the reaction  $Q$  value at  $-20$  MeV, which has been used to define “elastic scattering,” will include some contributions of strongly damped events, which, especially at these backwards angles, enhances the measured cross sections when compared with optical-model predictions. As a consequence of the definition of elastic scattering used in this work, the total reaction cross sections presented here do not include the inelastic and quasielastic scattering yields.

### C. Fission

Figure 3 shows the measured angular distributions of fission fragments with mass between 77.5 and 80 u and total kinetic energy between 110 and 120 MeV. These cuts were necessary because the angular acceptance of the detector system depends strongly on the mass and  $Q$  value of the reaction products. The total fission yields were derived by integrating over mass and  $Q$  value. The angle-integrated fission yields were obtained from the measured angular distributions assuming a  $1/\sin(\theta)$  dependence. This assumption is only valid in the limit of rapidly rotating systems; at energies close to the Coulomb barrier, the difference between the total fission cross sections obtained from fitting the measured angular distributions using the statistical model of fission and those obtained assuming a  $1/\sin(\theta)$  dependence can be as much as 25%.<sup>12</sup> However, our fission data do not cover the very forward and backward angles where the fission angular distributions obtained from the statistical model start deviating from a  $1/\sin(\theta)$  dependence, and therefore no attempts have been made to obtain the total fission yields using statistical-model fits.

The measured fission yields are tabulated in Table I. At the higher energies ( $E_{\text{lab}} \geq 225$  MeV) the errors in the fission yields are determined mainly by the uncertainties in the normalization procedure; at the lower energies, the uncertainties in the assumed  $1/\sin(\theta)$  angular dependence and the uncertainties in the width of the fission mass distribution discussed in Sec. III A dominate.

TABLE I. Total reaction cross sections, evaporation, fission, and calculated deep-inelastic scattering yields for  $^{64}\text{Ni} + ^{92}\text{Zr}$ .

$E_{\text{lab}}^a$ (MeV)	$\sigma_{\text{reac}}^b$ (mb)	$\sigma_{\text{evap}}^c$ (mb)	$\sigma_{\text{fiss}}$ (mb)	$\sigma_{\text{di}}^d$ (mb)
239.3±0.5	555±55	270±35	20±5	265±65
243.8±0.5	610±60	300±35	45±10	265±70
248.7±0.5	680±70	300±35	100±15	280±80
253.8±0.5	770±80	300±35	175±25	295±90
259.7±0.5	875±90	300±35	245±35	330±100
269.8±0.5	975±100	300±35	320±50	355±115
279.6±0.5	1050±100	300±35	405±60	345±125
289.2±0.5	1215±125	300±35	550±80	365±150
299.1±0.5	1345±135	300±35	740±110	305±175

<sup>a</sup>Corrected for energy loss in the target.

<sup>b</sup>Obtained from the measured “elastic scattering” angular distributions.

<sup>c</sup>From Ref. 4.

<sup>d</sup>Note that  $\sigma_{\text{di}} = \sigma_{\text{reac}} - \sigma_{\text{evap}} - \sigma_{\text{fiss}}$ .

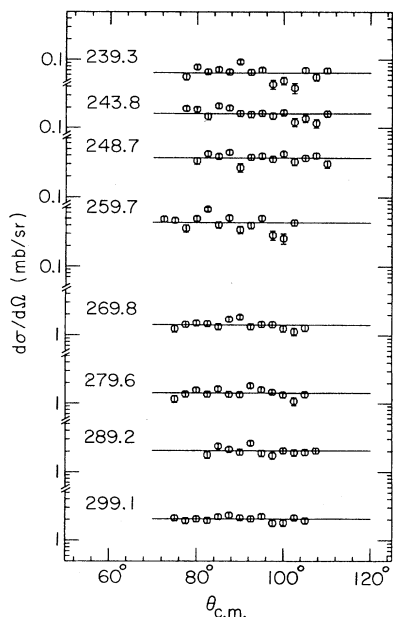


FIG. 3. Measured angular distributions of fission fragments at several bombarding energies (indicated are the laboratory energies in MeV). The lines indicate the fits to the angular distributions used to obtain the angle-integrated fission yields.

#### IV. DISCUSSION

##### A. Decomposition of the total reaction cross section

Figure 4 shows a comparison between the total reaction cross sections obtained from the measured “elastic scattering” angular distributions and the sum of the fission and the previously measured evaporation-residue yields<sup>4</sup> at various incident energies. A large fraction of the total reaction cross section is not accounted for by either the fission or the evaporation-residue yields. Similar observations have been made for the Ni+Sn and S+W systems,<sup>13,14</sup> where it was shown that deep-inelastic scattering accounts for the missing cross section. Accordingly, we have assumed that deep-inelastic scattering is also responsible for the missing fraction of the total reaction cross section for the Ni+Zr system. The calculated deep-inelastic scattering yields are tabulated in Table I. Figure 5 shows the strength of deep-inelastic scattering relative to the sum of the evaporation-residue, fission, and deep-inelastic scattering yields as a function of  $E_{c.m.}/E_{Coul}$  for  $^{58}\text{Ni} + ^{112,124}\text{Sn}$  (Ref. 13) and  $^{64}\text{Ni} + ^{92}\text{Zr}$ . The energy dependence of the relative strength of deep-inelastic scattering is remarkably similar for all three systems shown. This result can be regarded as an indication of the reliability of the analysis discussed in Sec. III.

In Ref. 13 it was shown that for  $^{58}\text{Ni} + ^{112,124}\text{Sn}$  the total kinetic energy of the deep-inelastic scattering fragments is consistent with a large deformation of each reaction product ( $\beta \approx 0.65$ ). If this is also the case for the Ni+Zr system, it indicates that during the initial stage of the reaction a large fraction of the available excitation energy is used to deform the system.

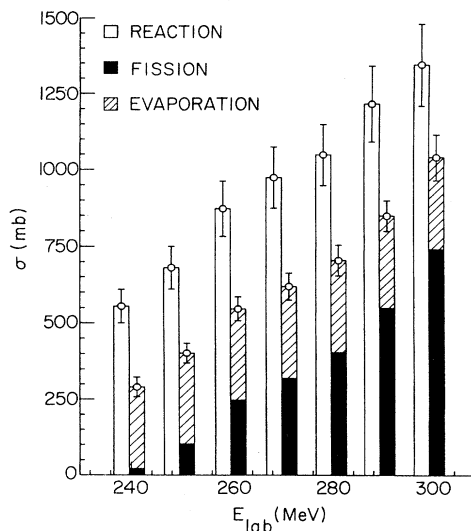


FIG. 4. Comparison between the total reaction cross sections obtained from the measured “elastic scattering” angular distributions and the sum of fission and previously measured evaporation-residue yields at various laboratory energies.

##### B. Comparison with statistical-model calculations

The measured fission yields combined with the results of previous studies of the Ni+Zr system<sup>1,4,5</sup> almost completely determine the set of input parameters used in statistical-model calculations with the code CASCADE.<sup>15</sup> The fission barriers of Sierk,<sup>16</sup> which incorporate the effects from the finite range of the nuclear force and the diffuseness of the nuclear surface, were used in these calculations. For the rotating liquid drop model masses, the Myers droplet parametrization with the Wigner term was used.<sup>17</sup> The level-density parameter  $a_n$  was chosen to be  $a_n = A/12$  ( $\text{MeV}^{-1}$ ) in order to reproduce the measured

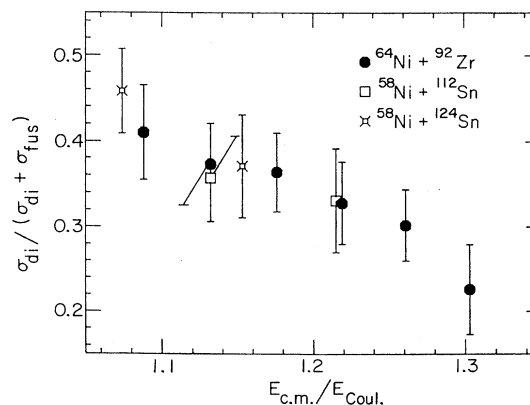


FIG. 5. Strength of deep-inelastic scattering relative to the sum of evaporation-residue, fission, and deep-inelastic scattering yields as a function of  $E_{c.m.}/E_{Coul}$  for  $^{58}\text{Ni} + ^{112}\text{Sn}$ ,  $^{58}\text{Ni} + ^{124}\text{Sn}$ , and  $^{64}\text{Ni} + ^{92}\text{Zr}$ .

neutron energy spectra discussed in Ref. 1. The ratio of level densities for fission and evaporation ( $a_f/a_n$ ) was assumed to be equal to 1. Measured yrast lines for nuclei in this mass region (extrapolated beyond the known maximum spin of  $43\hbar$ ) were used in the calculations, and included corrections for the odd-even and odd-odd nuclei. The code was modified to include enhanced, stretched  $E2$  transitions parallel to the yrast line and  $E1$  transitions through the giant dipole resonance, with the classical energy-weighted sum-rule strength.<sup>18</sup> The spin distribution of the compound nucleus was determined from the measured fusion yields and a given diffuseness  $\Delta l$ . This diffuseness  $\Delta l$  is the only free parameter in the calculations. Lesko *et al.*<sup>12</sup> have studied the competition between fission and evaporation for the Ni+Sn system in great detail and concluded that  $\Delta l = 7.5\hbar$  was required to fit the available data. Measurements of the shape of the spin distributions for the strongest evaporation-residue channels for the Ni+Zr system suggest  $\Delta l = 4\hbar$ .<sup>5</sup> Figures 6 and 7 show a comparison between the measured evaporation-residue and fission yields and CASCADE calculations (solid lines) with  $\Delta l = 4\hbar$  and  $\Delta l = 7.5\hbar$ , respectively. The dashed lines indicate the upper and lower limits of the calculated fission yields, corresponding to the upper and lower limits of the measured total fusion yields. For  $\Delta l = 7.5\hbar$  the slope of the fission excitation function is not well reproduced, and the fission yields at the lowest energies are clearly overestimated. For  $\Delta l = 4\hbar$ , the present data are in good agreement with the results of the CASCADE calculations.

The average neutron multiplicity  $\langle n \rangle$  discussed in Ref. 4 is defined as

$$\langle n \rangle = \frac{\sigma_{1n} + 2\sigma_{2n} + 3\sigma_{3n} + 4\sigma_{4n}}{\sigma_{1n} + \sigma_{2n} + \sigma_{3n} + \sigma_{4n}},$$

where  $\sigma_{1n}$ ,  $\sigma_{2n}$ ,  $\sigma_{3n}$ , and  $\sigma_{4n}$  are the yields for the  $1n$ ,  $2n$ ,  $3n$ , and  $4n$  channels, respectively. Figure 8 shows a comparison between the measured and calculated average neutron multiplicity<sup>4</sup> (solid line,  $\Delta l = 4\hbar$ ). The measured multiplicities are lower than the predicted values by about 0.35–0.55 neutrons. Changing the diffuseness of the compound nuclear spin distribution from  $4\hbar$  to  $7.5\hbar$  changes the calculated average neutron multiplicities by less than 0.05 neutrons. A further increase in the

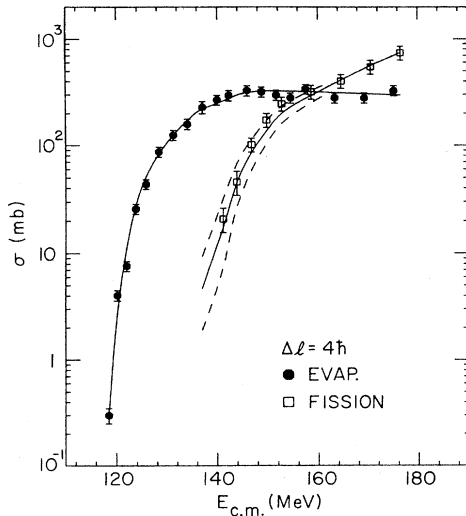


FIG. 6. Comparison between the measured evaporation-residue and fission yields (octagons and squares) and the results from statistical-model calculations (solid lines) using the code CASCADE for  $\Delta l = 4\hbar$ . The dashed lines indicate the error in the calculated fission yields induced by the uncertainties in the total fusion yield.

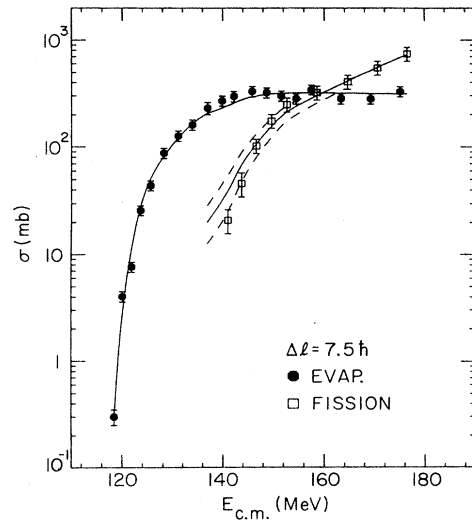


FIG. 7. Comparison between the measured evaporation-residue and fission yields (octagons and squares) and the results from statistical-model calculations (solid lines) using the code CASCADE for  $\Delta l = 7.5\hbar$ . The dashed lines indicate the error in the calculated fission yields induced by the uncertainties in the total fusion yield.

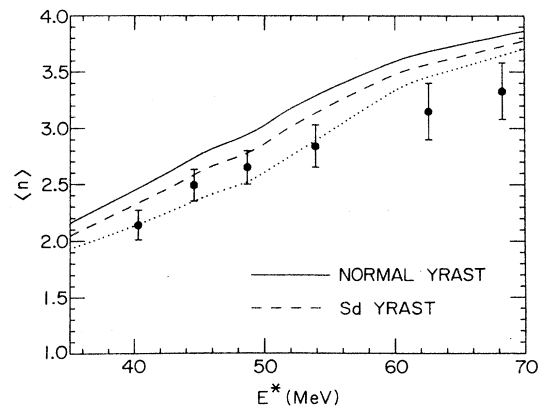


FIG. 8. Comparison between the neutron multiplicity measured as a function of the excitation energy in  $^{156}\text{Er}$  and the results of statistical-model calculations with CASCADE. The solid, dashed, and dotted lines shown are discussed in the text.

diffuseness of the spin distribution only minimally decreases the calculated average neutron multiplicities. However, it significantly increases the calculated fission cross sections and therefore can be ruled out on the basis of the measured fission yields.

It should be pointed out that the fusion cross section obtained by combining the results of the present experiment with the evaporation-residue cross sections of Ref. 4 can be used in conjunction with the spin distributions derived from gamma-ray multiplicity measurements.<sup>5</sup> The two data sets exist for the same beam energy of 237.5 MeV. They are not only complementary but also allow for a consistency check between the sets. If we adopt the form of the transmission coefficients  $T_l$  as

$$T_l = 1 / \{ 1 + \exp[(l - l_0) / \Delta l] \} ,$$

the absolute cross section for each partial wave ( $\sigma_l$ ) can be obtained from the measured fusion cross section ( $\sigma_{\text{fusion}}$ ) assuming  $\sigma_l = \pi \lambda^2 (2l + 1) T_l$  and  $\sum \sigma_l = \sigma_{\text{fusion}}$ . To calculate  $\sigma_l$  we have used the diffuseness  $\Delta l = 4\hbar$  of the spin distribution of the evaporation residues obtained from the crystal-ball measurement.<sup>5,19</sup> Figure 9 shows the comparison between the partial-wave distribution of the compound nucleus obtained from the crystal-ball measurement<sup>6</sup> and the fusion cross section at a compound nucleus excitation energy of 47 MeV. As can be seen from Fig. 9 the two sets of data are in good agreement. The  $l$  distribution from the crystal-ball measurement shown in Fig. 9 is revised with respect to that reported in Ref. 5; there is a systematic  $\sim 15\%$  increase in  $l$ , arising from a revised value of  $\Delta l$ , the average spin removed per photon.<sup>6</sup>

The spin-distribution data of Ref. 5 have been questioned on the basis of another experiment,<sup>8</sup> where indications for high- $l$  tails in the spin distributions have been found. The present data do not support the result of Ref. 8. Not only are the data of Ref. 5 (as modified by Ref. 6)

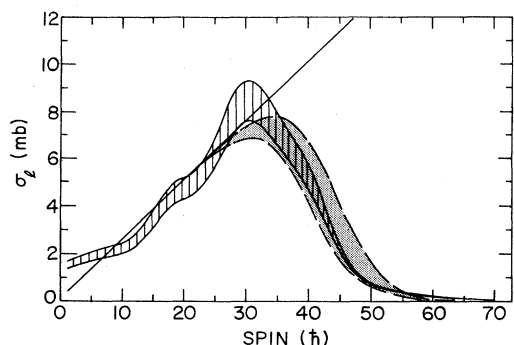


FIG. 9. Comparison of the compound-nucleus spin distribution obtained at the Heidelberg-Darmstadt crystal ball (horizontal lines) and the distribution deduced from the measured fusion cross sections (shaded area). The data are for the  $^{64}\text{Ni} + ^{92}\text{Zr}$  reaction at 237.5 MeV. The lines encompassing the shaded and lined areas represent normalization to  $\sigma_{\text{er}} = \sigma_{\text{meas}}$  and  $0.85 \sigma_{\text{meas}}$ , representing half of the uncertainty in the measured evaporation-residue cross section.

and the present fusion cross section in excellent agreement, we have also shown that any increase in the value of the diffuseness parameter used in the CASCADE calculations results in a poorer description of the fission–evaporation-residue competition. Hence, we conclude that the very high- $l$  tails implied by Ref. 8 are not present. In any event such tails have little effect on the evaporation-residue yields, since for  $l \geq 55\hbar$  the ratio  $\sigma_{\text{fission}} / \sigma_{\text{er}}$  increases rapidly with  $l$  (according to the CASCADE calculations which reproduce the fission cross sections).

### C. Superdeformation

The results of the CASCADE calculations discussed in Sec. IV B suggest that the discrepancy between the measured and calculated average neutron multiplicities cannot be resolved by any change in the spin distribution of the compound nucleus. Since the neutron suppression cannot be attributed to other simple explanations—uncertainties in the yrast line, neutron kinetic energy, or the  $\gamma$  strength function—we are left with having to pursue more exotic explanations. It appears that not all of the internal energy is available as “heat” for neutron emission. A plausible explanation is that some of the energy is tied up in deformation, implying that the relaxation from the highly deformed initial shape proceeds on a time scale comparable to that for neutron emission, i.e.,  $10^{-19} - 10^{17}$  s. This slow relaxation process could be due to an as yet unexplained dynamic effect in the nuclear dissipation. An alternative picture, first proposed in Ref. 1, is that the compound nucleus is trapped in a superdeformed minimum well during the shape relaxation process. Theory predicts the occurrence of such a well in the relevant  $^{154-156}\text{Er}$  nuclei at high spin, and superdeformed discrete line bands have been recently discovered<sup>20-22</sup> in this mass region.

In order to study the effect of superdeformation on the neutron multiplicities, we have replaced the normal yrast line used in the CASCADE calculations discussed in Sec. IV B with an elevated yrast line describing the superdeformed band recently observed in  $^{151}\text{Dy}$ .<sup>22</sup> Figure 10 shows that the measured and calculated evaporation-residue and fission yields are in reasonable agreement. The calculated average neutron multiplicities (dashed line in Fig. 8) are lower than those discussed in Sec. IV B by 0.1–0.2 neutrons, but still overestimate the measured neutron multiplicities somewhat. The calculated neutron multiplicities can be further decreased by increasing the moment of inertia of the superdeformed yrast line (25% increase, dotted curve in Fig. 8), but in this case the measured competition between fission and evaporation is not reproduced by the CASCADE calculations.

It may appear that the interpretation of the inhibition of neutron emission in terms of superdeformation is not consistent with the observation that the strength of transitions in the superdeformed bands is at most 1% of the estimated total evaporation-residue yields.<sup>20-22</sup> Indeed, this would be so if the trapping time in the secondary minimum persists for times comparable to those for decay along the superdeformed bands ( $10^{-14} - 10^{13}$  s). How-

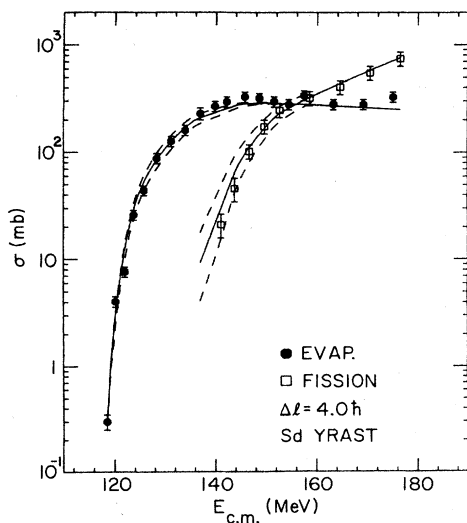


FIG. 10. Comparison between the measured evaporation-residue and fission yields and the results of statistical-model calculations with the code CASCADE assuming decay along a superdeformed yrast line.

ever, since in the compound nucleus the energy above the barrier separating the superdeformed and normal states is estimated to be around 28 MeV, one could not expect trapping for such a long time. Thus, if trapping is indeed the reason for neutron suppression, this suggests that it persists only for  $10^{-17}$ – $10^{-16}$  s, when statistical  $\gamma$  emis-

sion begins to cool the nucleus, thereby not allowing further neutron emission. Indeed, the measured  $\gamma$ -ray sum energies in the  $^{64}\text{Ni} + ^{92}\text{Zr}$  fusion reaction are larger than what would customarily be obtained.<sup>23</sup>

## V. SUMMARY

We have measured the fission yields for  $^{64}\text{Ni} + ^{92}\text{Zr}$  at bombarding energies between 1.05 and 1.30 times the Coulomb barrier. The competition between fission and light-particle evaporation is reproduced by statistical-model calculations with the code CASCADE and defines the diffuseness of the spin distribution of the compound nucleus to be  $\Delta I = 4\hbar$ . The calculated neutron multiplicities still overestimate the previously measured multiplicities. The difference can be reduced by replacing the normal yrast line used in the calculations with an elevated yrast line, suggesting that a fraction of the excitation energy is tied up in deformation during the neutron emission time.

## ACKNOWLEDGMENTS

We express our gratitude to the accelerator crew of ATLAS for providing us with  $^{64}\text{Ni}$  beams of excellent quality. This work was supported by the U.S. Department of Energy, Nuclear Physics Division, under Contract No. W-31-109-Eng-38.

\*Present address: GSI, D-6100 Darmstadt 11, Federal Republic of Germany.

†Present address: Tsinghua University, Beijing, People's Republic of China.

<sup>1</sup>W. Kühn, P. Chowdhury, R. V. F. Janssens, T. L. Khoo, F. Haas, J. Kasagi, and R. M. Ronningen, Phys. Rev. Lett. **51**, 1858 (1983).

<sup>2</sup>C. Cabot, H. Gauvin, H. Sergolle, P. Aguer, G. Bastin, J. P. Thibaud, H. Delagrangé, and Y. Patin, Z. Phys. A **322**, 393 (1985).

<sup>3</sup>P. M. Stwertka, T. M. Cormier, M. Herman, and N. G. Nicolis, Phys. Lett. **150B**, 91 (1985).

<sup>4</sup>R. V. F. Janssens, R. Holzmann, W. Henning, T. L. Khoo, K. T. Lesko, G. S. F. Stephans, D. C. Radford, A. M. van den Berg, W. Kühn, and R. M. Ronningen, Phys. Lett. B **181**, 16 (1986).

<sup>5</sup>A. Ruckelshausen, R. D. Fischer, W. Kühn, V. Metag, R. Mühlhans, R. Novotny, T. L. Khoo, R. V. F. Janssens, H. Gröger, D. Habs, H. W. Heyng, R. Repnow, D. Schwalm, G. Duchène, R. M. Freeman, B. Haas, F. Haas, S. Hlavac, and R. S. Simon, Phys. Rev. Lett. **56**, 2356 (1986).

<sup>6</sup>A. Ruckelshausen, B. Haas, D. Habs, R. V. F. Janssens, T. L. Khoo, W. Kühn, V. Metag, D. Schwalm, and R. S. Simon, Phys. Rev. Lett. **58**, 1584 (1987).

<sup>7</sup>S. Henss, A. Ruckelshausen, R. D. Fischer, W. Kühn, V. Metag, R. Novotny, R. V. F. Janssens, T. L. Khoo, D. Habs, D. Schwalm, D. Freeman, D. Duchène, B. Haas, F. Haas, S.

Hlavac, and R. S. Simon, Phys. Rev. Lett. **60**, 11 (1988).

<sup>8</sup>D. J. G. Love, P. J. Bishop, A. Kirwan, P. J. Nolan, D. J. Thornley, A. H. Nelson, and P. J. Twin, Phys. Rev. Lett. **57**, 551 (1986).

<sup>9</sup>R. Pardo, B. E. Clift, P. DenHartog, D. Kovar, W. Kutschera, and K. E. Rehm, Nucl. Instrum. Methods (to be published).

<sup>10</sup>V. E. Viola, Jr., Nucl. Data Sec. A **1**, 391 (1966).

<sup>11</sup>V. M. Strutinski, Zh. Eksp. Teor. Fiz. **46**, 1907 (1964) [Sov. Phys.—JETP **18**, 1305 (1964)].

<sup>12</sup>K. T. Lesko, W. Henning, K. E. Rehm, G. Rosner, J. P. Schiffer, G. S. F. Stephans, and W. S. Freeman, Phys. Rev. C **34**, 2155 (1986).

<sup>13</sup>F. L. H. Wolfs, Phys. Rev. C **36**, 1379 (1987).

<sup>14</sup>J. G. Keller, B. B. Back, B. G. Glagola, D. Henderson, S. B. Kaufman, S. J. Sanders, R. H. Siemssen, F. Videbaek, B. D. Wilkins, and A. Worsham, Phys. Rev. C **36**, 1364 (1987).

<sup>15</sup>F. Pühlhofer, Nucl. Phys. A **280**, 267 (1977).

<sup>16</sup>H. J. Krappe, J. R. Nix, and A. J. Sierk, Phys. Rev. C **20**, 992 (1979).

<sup>17</sup>W. D. Myers, *Droplet Model of the Atomic Nucleus*, (IFI/Plenum, New York, 1977).

<sup>18</sup>K. A. Snover, Annu. Rev. Nucl. Part. Sci. **36**, 545 (1986).

<sup>19</sup>T. L. Khoo, in *Weak and Electric Interactions in Nuclei*, Proceedings of the International Symposium, Heidelberg, 1986, edited by H. V. Klapdor (Springer, New York, 1987).

<sup>20</sup>P. J. Twin, B. M. Nyakó, A. H. Nelson, J. Simpson, M. A. Bentley, H. W. Cranmer-Gordon, P. D. Forsyth, D. Howe, A.

- R. Mokhtar, J. D. Morrison, J. F. Sharpey-Schafer, and G. Sletten, *Phys. Rev. Lett.* **57**, 811 (1986).
- <sup>21</sup>B. Haas, P. Taras, S. Flibotte, F. Banville, J. Gascon, S. Cournoyer, S. Monaro, N. Nadon, D. Prévost, D. Thibault, J. K. Johansson, D. M. Tucker, J. C. Waddington, H. R. Andrews, G. C. Ball, D. Horn, D. C. Radford, D. Ward, C. St. Pierre, and J. Dudek, *Phys. Rev. Lett.* **60**, 503 (1988).
- <sup>22</sup>G.-E. Rathke, R. V. F. Janssens, M. W. Drigert, I. Ahmad, K. Beard, R. R. Chasman, U. Garg, M. Hass, T. L. Khoo, H.-J. Körner, W. C. Ma, S. Pilotte, P. Taras, and F. L. H. Wolfs, *Phys. Lett. B* **209**, 177 (1988).
- <sup>23</sup>A. Ruckelshausen, Ph.D. thesis, University of Giessen, 1987.